Table 2 Abbreviations and units

Variables: italic font

Abbreviation	*Description*	*Units or not applicable*
B_{max}	Density of receptors *in vitro*	Often pmol per mg protein
B_{avail}	Density of receptors available to bind radioligand *in vivo*	molar (often nmol · L^{-1}, i.e., nmol receptor per 1,000 cm^{-3} tissue)
BP	*In vitro* binding potential	unitless
BP_F, BP_P, and BP_{ND}	*In vivo* binding potentials (see Table 1)	unitless or mL · cm^{-3}
C	Concentration—as in C_P, C_{ND}, C_S, C_{FT}, and C_{NS}	Bq · mL^{-1} or molar
ΔBP_F, ΔBP_P, and ΔBP_{ND}	Percent change in binding potential caused by occupancy or displacement	%
f_P	Free fraction in plasma	unitless[a]
f_{ND}	Free fraction in nondisplaceable compartment	unitless[a]
K_1	Rate constant for transfer from arterial plasma to tissue	mL · cm^{-3} · min^{-1}
k_2, k_3, k_4	Rate constants	min^{-1}
$K_D = k_{off}/k_{on}$	Dissociation constant	molar (often nmol · L^{-1})
k_{off}	*In vitro* dissociation rate constant	min^{-1}
k_{on}	*In vitro* association rate constant	nmol · L^{-1} · min^{-1}
V_T, V_S, V_{ND}, and V_{NS}	Volumes of distribution expressed relative to total plasma ligand concentration C_P	mL · cm^{-3}

Subscripts: normal font

Abbreviation	*Description*
FP	'Free' radioligand in plasma, as in C_{FP}
FT	'Free' radioligand in tissue, as in C_{FT}
ND	Nondisplaceable tissue uptake, as in V_{ND} and C_{ND}
NS	Nonspecific ligand binding, as in V_{NS} and C_{NS}
P	Plasma free plus protein bound, as in C_P
S	Specific (i.e., receptor) bound ligand, as in V_S and C_S
T	Total radioligand in tissue (i.e., free plus bound), as in V_T and C_T

[a]Free fractions include correction for aqueous fraction in plasma and tissue (see text for details).

For example, in clinical pharmacology, the effects of drugs are related to the percentage of receptor sites occupied by the drug. This receptor occupancy can be defined as

$$\left(1 - \frac{B_{avail}(\text{treatment})}{B_{avail}(\text{baseline})}\right) \times 100\% \qquad (23)$$

where B_{avail}(treatment) is the density of available receptors under the drug treatment condition. The *in vivo* experiment can be used to measure a percentage change in binding potential owing to reduced receptor availability and can be measured with BP_F, BP_P, or BP_{ND}:

$$\Delta BP_X = \left(1 - \frac{BP_X(\text{treatment})}{BP_X(\text{baseline})}\right) \times 100\% \qquad (24)$$

where BP_X denotes one of the binding potential formulations. The percent change in BP_X and receptor occupancy will be equivalent under ideal conditions if the other parameters contributing to BP_X (e.g., K_D or f_P) do not change between control and treatment conditions. In addition, if ΔBP_X is not asymptotic to 100% at progressively higher drug concentrations, then some correction is necessary to estimate receptor occupancy from ΔBP_X.

Summary

The field of *in vivo* radioligand imaging has generated several different nomenclatures and abbreviations (see Table 2). We did not review these variations, so as not to confuse the reader. We think that these varying nomenclatures are confusing and detrimental to the field. Thus, we recommend the consensus nomenclature in this manuscript to improve the clarity of communications. We provide terminology for only two compartmental models (i.e., one- and two-tissue) and recognize that additional models and new discoveries will require additional terms. We hope that this basic structure will provide a useful pattern for future additions to this nomenclature.

Disclaimer

Although this article was written as part of Dr Innis's official duties as a government employee, the views expressed in this article do not necessarily represent those of NIMH, NIH, HHS, or the United States Government.

References

Delforge J, Syrota A, Bendriem B (1996) Concept of reaction volume in the *in vivo* ligand–receptor model. *J Nucl Med* 37:118–25

Gunn RN, Lammertsma AA, Hume SP, Cunningham VJ (1997) Parametric imaging of ligand–receptor binding in PET using a simplified reference region model. *Neuroimage* 6:279–87

Koeppe RA, Holthoff VA, Frey KA, Kilbourn MR, Kuhl DE (1991) Compartmental analysis of [^{11}C]flumazenil kinetics for the estimation of ligand transport rate and receptor distribution using positron emission tomography. *J Cereb Blood Flow Metab* 11: 735–44

Lammertsma AA, Hume SP (1996) Simplified reference tissue model for PET receptor studies. *NeuroImage* 4:153–8

Laruelle M, Abi-Dargham A, Al-Tikriti MS, Baldwin RM, Zea-Ponce Y, Zoghbi SS, Charney DS, Hoffer PB, Innis RB (1994) SPECT quantification of [^{123}I] iomazenil binding to benzodiazepine receptors in nonhuman primates. II. Equilibrium analysis of constant infusion experiments and correlation with *in vitro* parameters. *J Cereb Blood Flow Metab* 14: 453–65

Laruelle M (2000) Imaging synaptic neurotransmission with *in vivo* binding competition techniques: a critical review. *J Cereb Blood Flow Metab* 20:423–51

Lassen NA (1992) Neuroreceptor quantitation *in vivo* by the steady state principle using constant infusion or bolus injection of radioactive tracers. *J Cereb Blood Flow Metab* 12:709–16

Logan J, Fowler JS, Volkow ND, Wang GJ, Ding YS, Alexoff DL (1996) Distribution volume ratios without blood sampling from graphical analysis of PET data. *J Cereb Blood Flow Metab* 16:834–40

Mintun MA, Raichle ME, Kilbourn MR, Wooten GF, Welch MJ (1984) A quantitative model for the *in vivo* assessment of drug binding sites with positron emission tomography. *Ann Neurol* 15:217–27

Robertson MW, Leslie CA, Bennett JP (1991) Apparent synaptic dopamine deficiency induced by withdrawal from chronic cocaine treatment. *Brain Res* 538:337–9

Taylor BN (1995) *Guide for the use of the international system of units (SI).* Gaithersburg, MD: National Institute of Standards and Technology http://physics.nist.gov/cuu/pdf/sp.811.pdf

Votaw JR, Kessler RM, de Paulis T (1993) Failure of the three compartment model to describe the pharmacokinetics in brain of a high affinity substituted benzamide. *Synapse* 15:177–90

Delayed Postischemic Treatment With Fluvastatin Improved Cognitive Impairment After Stroke in Rats

Munehisa Shimamura, MD, PhD; Naoyuki Sato, MD, PhD; Masataka Sata, MD, PhD; Hitomi Kurinami, MD; Daisuke Takeuchi, MD; Kouji Wakayama, MD; Takuya Hayashi, MD, PhD; Hidehiro Iida, MD, PhD; Ryuichi Morishita, MD, PhD

Background and Purposes—Recent clinical evidences indicate that statins may have beneficial effects on the functional recovery after ischemic stroke. However, the effect of delayed postischemic treatment with statins is still unclear. In the present study, we evaluated the effects of fluvastatin in the chronic stage of cerebral infarction in a rat model.

Methods—Rats exposed to permanent middle cerebral artery occlusion were treated for 3 months with fluvastatin beginning from 7 days after stroke. MRI, behavioral analysis, and immunohistochemistry were performed.

Results—Two months of treatment with fluvastatin showed the significant recovery in spatial learning without the decrease in serum total cholesterol level and worsening of infarction. Microangiography showed a significant increase in capillary density in the peri-infarct region in fluvastatin-treated rats after 3 months of treatment. Consistently, BrdU/CD31-positive cells were significantly increased in fluvastatin-treated rats after 7 days of treatment. MAP1B-positive neurites were also increased in the peri-infarct region in fluvastatin-treated rats. In addition, rats treated with fluvastatin showed the reduction of superoxide anion after 7 days of treatment and the reduction of Aβ deposits in the thalamic nuclei after 3 months of treatment.

Conclusions—Thus, delayed postischemic administration of fluvastatin had beneficial effects on the recovery of cognitive function without affecting the infarction size after ischemic stroke. Pleiotropic effects of fluvastatin, such as angiogenesis, neuritogenesis, and inhibition of superoxide production and Aβ deposition, might be associated with a favorable outcome. (***Stroke*. 2007;38:3251-3258.)**

Key Words: angiogenesis ■ cerebral infarct ■ microcirculation ■ statins

Despite conflicting data correlating cholesterol level with stroke, 2 early trials of HMG-CoA reductase inhibitors (statins) in patients after myocardial infarction patients showed a reduction in stroke risk as a secondary end point.[1] A meta-analysis of 9 statin intervention trials, which enrolled patients with coronary artery disease or those at high risk for coronary disease, demonstrated a 21% relative risk reduction for stroke after 5 years of treatment.[2] Another clinical evidence suggests that the commencement of statins within 4 weeks of a stroke results in a favorable 90-day outcome.[3] To clarify the effects of postischemic statin treatment, previous studies in which atorvastatin was started 1 day after stroke in rodents showed improvement of sensory motor deficit through induction of angiogenesis, neurogenesis, and synaptogenesis.[4,5] These pleiotropic effects of statins were shown to be the result of induction of vascular endothelial growth factor or brain-derived neurotrophic factor.[4] Additionally, the microvascular dysfunction in the posttreatment of stroke with recombinant human tissue-type plasminogen activator could be reduced by statins in rodent model.[6] However, the effect of delayed treatment with statins after ischemic stroke is still unknown. From this viewpoint, we investigated whether chronic statin treatment beginning 7 days after ischemic stroke had influences on neurological deficits and pathophysiology after the permanent middle cerebral artery occlusion (MCAo) model in rats.

Materials and Methods

Surgical Procedure

Male Wistar rats (270 to 300 grams; Charles River; Kanagawa, Japan) were used in this study. The right MCA was occluded by placement of poly-L-lysine–coated 4-0 nylon, as described previously.[7]

Protocol for Treatment and Behavioral Tests

Ten rats were only anesthetized (sham operation) and 32 rats were subjected to MCAo (day 1). Based on neuromuscular function on day 7, the rats were divided equally into saline-treated (n=16) or fluvastatin-treated (n=16) groups. Fluvastatin (5 mg/kg per day;

Received February 14, 2007; final revision received April 27, 2007; accepted May 30, 2007.

From Department of Advanced Clinical Science and Therapeutics (M.S., M.Sata, K.W.), Graduate School of Medicine, the University of Tokyo, Japan; Department of Clinical Gene Therapy (N.S., H.K., D.T., R.M.), Graduate School of Medicine, Osaka University, Japan; Department of Investigative Radiology (T.H., H.I.), National Cardiovascular Center, Research Institute, Japan.

Correspondence to Ryuichi Morishita, MD, PhD, Professor, Division of Clinical Gene Therapy, Graduate School of Medicine, Osaka University, 2-2 Yamada-oka, Suita 565-0871, Japan. E-mail morishit@cgt.med.osaka-u.ac.jp

***Stroke* is available at http://stroke.ahajournals.org** **DOI: 10.1161/STROKEAHA.107.485045**

provided by Novartis Pharma) or saline was given by gavage from day 7 to 100. We chose the dose (5 mg/kg per day), because a previous report showed that this dose could effectively induce angiogenesis in ischemic limb.[8] On day 55, neuromuscular function and locomotor activity were evaluated in the surviving rats. Then, cognitive function was examined by Morris water maze from day 56 to 63, because the effects of neuronal regeneration could be detected not in the early stage but in the chronic stage of ischemic brain such as 49 to 53 days after the insult.[9] On day 96, MRI was performed. On day 100, microangiography was performed.

MRI

High-resolution T1-weighted fast spin echo sequence images (repetition time [TR]=1500 ms; echo time [TE]=10.3 ms; field of view [FOV]=4× 3 cm; matrix=256×192; slice thickness=1.5 mm; slice gap=0.5 mm; number of slices=16; number of excitation=10; total time=9.39 min) were obtained using a 3-T MRI scanner (Signa LX VAH/I; GE).

Sensory Motor Deficit and Locomotor Activity

Although there are various batteries for testing sensory motor deficit, we used a simple protocol.[10] For forelimb flexion, rats were held by the tail on a flat surface. Paralysis of the forelimbs was evaluated by the degree of left forelimb flexion. For torso twisting, rats were held by the tail on a flat surface. The degree of body rotation was checked. For lateral push, rats were pushed either left or right. Rats with right MCA occlusion showed weak or no resistance against a left push. For hind limb placement, one hind limb was removed from the surface. Rats with right MCA occlusion showed delayed or no replacement of the hind limb when it was removed from the surface.

Spontaneous activity was measured via the open field (0.69 m^2). We set the sensor, which also put beams on the field, at 30 cm above the field. The number of count, which is when the animal crosses the beam, was measured for 30 minutes.

Morris Water Maze Task

A cylindrical tank 1.5 m in diameter was filled with water (25°C), and a transparent platform 15 cm in diameter was placed at a fixed position in the center of 1 of the 4 quadrants (O'Hara & Co, Ltd). In the hidden platform trials, we performed the tests 4 times per day for 4 days. When the rat could not reach the platform, the latency was set at 60 sec. In the visible platform trials, the tests were performed 4 times per day for 4 days. The acquired data were averaged per day.

Evaluation of Capillary Density

Using a recently developed microangiographic technique,[11] capillary density and blood–brain barrier leakage were evaluated in the cerebral cortex after MCA occlusion. The area or length of vessels was analyzed with an angiogenesis image analyzer (version 1.0; Kurabo).

Immunohistochemical Study: Bromodeoxyuridine Labeling

To identify newly formed DNA, saline-treated (n=5) and fluvastatin-treated (n=5) rats received injections of bromodeoxyuridine (BrdU, 50 mg/kg; Sigma-Aldrich, Saint Louis, Mo) intraperitoneally starting on day 7 twice per day until day 13. Rats were euthanized on day 14. After the sections (8-μm thickness) was fixed in 10% formaldehyde/MeOH neutral buffer solution and blocked, they were incubated with mouse monoclonal anti-rat CD31 antibody (1:100; BD Biosciences; San Jose, Calif), goat polyclonal anti-doublecortin (anti-DCX; Santa Cruz) antibody (1:100; Santa Cruz, Calif), mouse monoclonal anti-NeuN antibody (1:1000; Chemicon, Temecula, Calif), or mouse monoclonal anti-MAP1B antibody (1:100; Sigma-Aldrich), followed by anti-mouse goat fluorescent antibody (1:1000 for NeuN and MAP1B, 1:400 for CD31, Alexa Flour 546, Molecular Probes; Eugene, Ore) or anti-goat donkey fluorescent antibody (1:1000 for DCX Alexa Fluor 546). For double immunostaining, these sections were fixed again and incubated in 2 N HCl at 37°C for 30 minutes. After blocking, they were incubated with rat monoclonal anti-BrdU antibody (1:200; Abcam, Cambridge, UK) followed by anti-rat goat fluorescent antibody (1:1000, Alexa Fluor 488). For immunohistochemical staining for Aβ, sections were pretreated for 30 minutes with hot (85°C) citrate buffer as described before.[12] Confocal images were acquired using an FV-300 (Olympus).

Table. Infarction Volume Calculated by MRI, Blood Pressure, and Serum Total Cholesterol

	Sham	MCAo+S	MCAo+F	*P*
Infarction volume in total rats (mm^3)	...	283.8±23.9	278.4±26.4	0.851
Type of infarction in Figure 1a (N of rats)				0.828
A	...	12	11	...
B	...	3	3	...
C	...	1	2	...
Infarction volume (mm^3) in type A rats	...	322.8±15.0	327.0±18.8	0.758
Systolic blood pressure (mm Hg) in type A rats				
Day 7	116.1±5.4	123.7±6.0	115.5±7.3	0.654
Day 56	146.5±4.7	148.3±2.7	136.1±5.2	0.132
Serum total cholesterol (mg/dl) in type A rats on day 56	85.9±5.6	75.3±3.5	73.5±2.7	0.949

Type A, low-intensity area seen in the dorsolateral and lateral portions of the neocortex and the entire caudate putamen; type B, low-intensity area seen in the dorsolateral and lateral portions of the neocortex and in part of the caudate putamen; type C, low-intensity area seen in part of the lateral neocortex and caudate putamen. MCAo+S, saline-treated rats after MCAo; MCAo+F, fluvastatin-treated rats after MCAo.

P, saline vs fluvastatin.

Quantitative Histological Analysis

To quantify the immunoreactivity for MAP1B and Aβ, the acquired image was analyzed by Image J (version 1.32; NIH).

Detection of Superoxide Anion in Brain Sections

Superoxide anion was detected on day 14 as described previously.[13] Because intact cortex showed red fluorescence, we calculated the ratio of fluorescence as follows: ratio of fluorescence=[fluorescence intensity in ischemic core or peri-infarct region]/[fluorescence intensity in intact region].

Statistical Analysis

All values are expressed as mean±SEM. To analyze the differences in the type of cerebral infarction, χ^2 test was performed. The latency, path length, and mean speed in Morris water maze and sensory motor deficits were analyzed by a 2-factor repeated-measure ANOVA. Post hoc analyses were performed, and the Scheffe test was applied to control the inflation in type I error. The value of the serum total cholesterol, the blood pressure, and the spontaneous activity was analyzed by Scheffe rules. The differences in the immunohistochemistry and the volume of infarction were assessed by Mann–Whitney *U* analyses. In all cases, $P<0.05$ was considered significant.

Results

Effects of Fluvastatin on Cognitive Impairment

To confirm the severity of cerebral infarction, all rats were examined by T1-weighted MRI after 89 days of treatment. Although the total volume of infarction calculated in T1-weighted images was not different between rats treated with

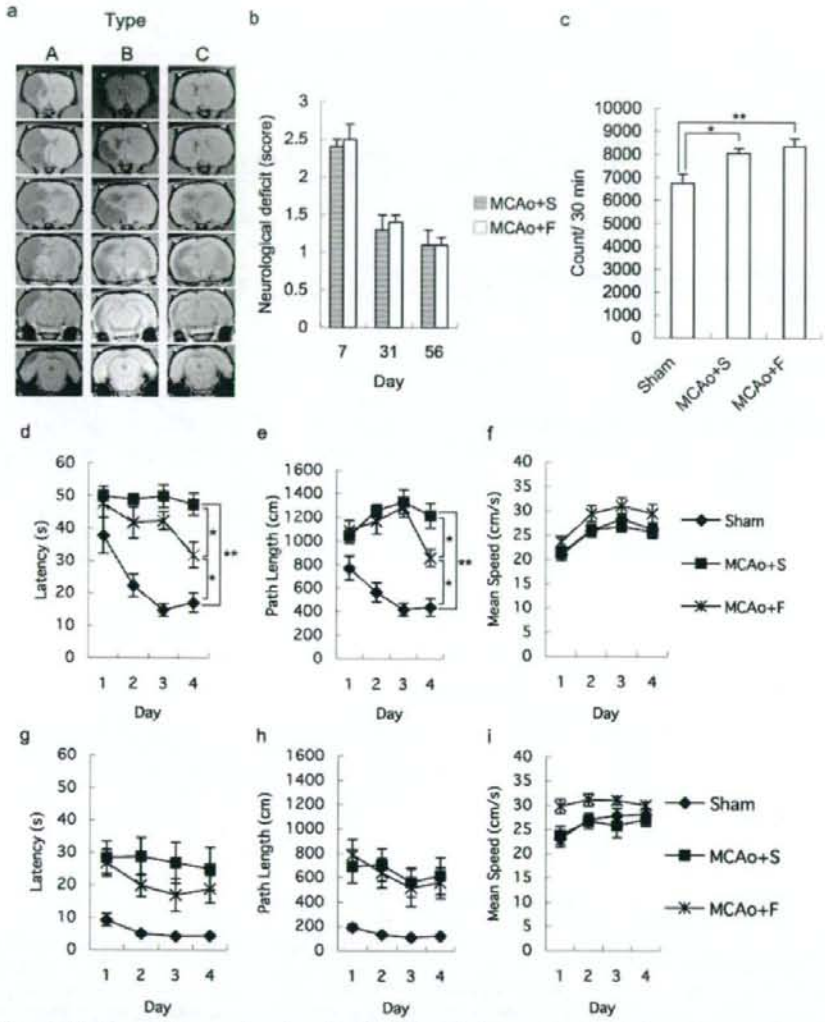

Figure 1. Typical T1-weighted image of coronal section of rat brain (a). The images were divided into 3 groups. Type A, low-intensity area seen in the dorsolateral and lateral portions of neocortex and the entire caudoputamen; type B, low-intensity area seen in the dorsolateral and lateral portions of neocortex and in part of the caudatoputamen; and type C, high-intensity area seen in part of the lateral neocortex and caudatoputamen. Sensory motor deficit (b). Spontaneous locomotor activity (c). Hidden platform test in Morris water maze. Each figure showed latency (d), path length (e), and mean speed (f). Days 1 to 4 indicate the trial day in the hidden platform test (56 to 59 days after middle cerebral artery occlusion). Visible platform test in Morris water maze. Each figure showed latency (g), path length (h), and mean speed (i). Days 1 to 4 indicate the day in the visible platform test (60 to 63 days after middle cerebral artery occlusion). MCAo+S indicates rats treated with saline after middle cerebral artery occlusion; MCAo+F, rats treated with fluvastatin after middle cerebral artery occlusion.

saline and fluvastatin (Table), the pattern of cerebral infarction was divided into 3 groups: type A, low-intensity area seen in the dorsolateral and lateral portions of the neocortex and the entire caudate putamen; type B, low-intensity area seen in the dorsolateral and lateral portions of the neocortex and in part of the caudate putamen; type C, low-intensity area seen in part of the lateral neocortex and caudate putamen (Figure 1a). In type C, most of the lateral neocortex was intact. To exclude the influence of the pattern of cerebral infarction on cognitive function, we focused on type A rats in the present study. The volume of cerebral infarction in type A rats was not different between the groups (Table). Blood pressure and serum total cholesterol also showed no difference among the groups (Table).

Sensory motor deficit had spontaneously recovered to some extent by 8 weeks in both groups, and there was no difference (Figure 1b). Locomotor activity in rats subjected to MCAo was increased as compared with that in sham-operated rats, as described before,[14] but there was no significant difference between fluvastatin-treated and saline-treated rats (Figure 1c). In Morris water maze (Figure 1d-i), which examines spatial learning, there were significant differences

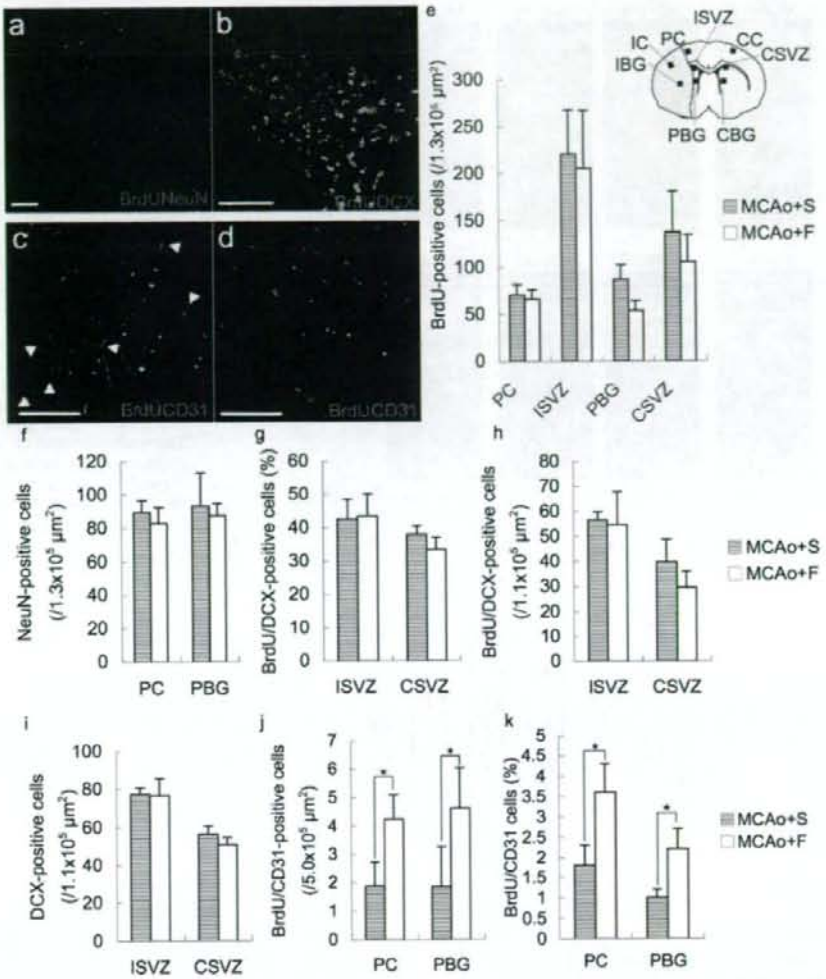

Figure 2. Representative images of immunohistochemical staining on day 14. Rats treated with fluvastatin (a through c), rats treated with saline (d). Although BrdU-positive cells were observed in the peri-infarct cortex (a), peri-infarct basal ganglia, and subventricular zone, these cells did not express NeuN (a), but expressed DCX in the subventricular zone (b). Fluvastatin-treated rats showed some BrdU/CD31-positive cells (arrows, c), although most BrdU-positive cells were negative for CD31 in saline-treated rats (d). The number of BrdU-positive cells (e), NeuN-positive cells (f), BrdU/DCX-positive cells (h), DCX-positive cells (i), and BrdU/CD31-positive cells (j); the percentage of BrdU/DCX-positive cells (g) or BrdU/CD31 cells (k) in total BrdU-positive cells. PC indicates peri-infarct cortex; PBG, peri-infarct basal ganglia; IC, infarcted cortex; IBG, ischemic basal ganglia; ISVZ, subventricular zone on infarcted side; CC, contralateral cortex, CSVZ, subventricular zone on contralateral side; CBG, contralateral basal ganglia (n=5 in each group, $^*P<0.05$, bar=100 μm).

in the latency and path length in hidden platform test among the groups (supplemental Table I, available online at http://stroke.ahajournals.org). A significant difference was observed on day 4 between fluvastatin-treated and saline-treated rats (supplemental Table I). Also, there was a significant difference between sham and saline-treated rats (supplemental Table I). There was no significant difference both in swimming speed and visible platform test, which excluded the possible influence of visual loss, sensory motor deficit, and motivation on the results.[15] These data suggest that impaired spatial learning was improved by fluvastatin.

Histological Changes by Fluvastatin

Next, we studied whether fluvastatin had some influences on the histology. Initially, we focused on neurogenesis and angiogenesis. To examine neurogenesis, we measured BrdU-incorporated cells after injecting BrdU from day 7 to day 13. Although BrdU-positive cells were observed in the subventricular zone and peri-infarct region (Figure 2a to 2d), the total number did not differ between the groups (Figure 2e). Similarly, the density of NeuN-positive cells, as a marker of adult neurons, also did not differ between the groups (Figure 2f), whereas there were no BrdU/NeuN-positive cells in the

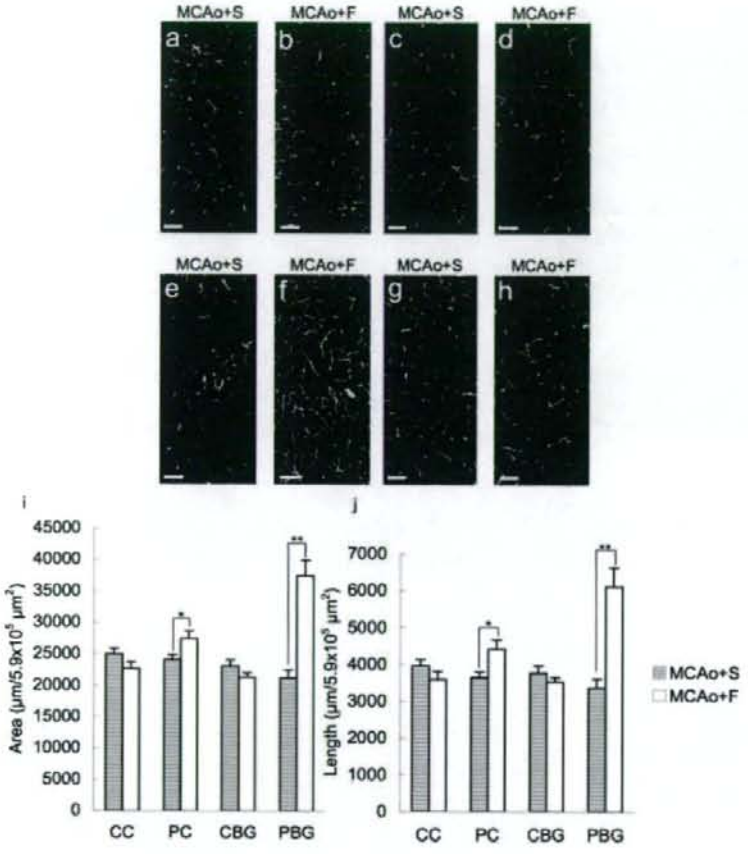

Figure 3. Microangiographic images using albumin-fluorescence isothiocyanate on day 100: (a and b) peri-infarct cortex; (c and d) contralateral cortex; (e and f) peri-infarct basal ganglia; (g and h) contralateral basal ganglia (bar=100 μm). Quantitative analysis (i and j) of microangiography. Rats treated with fluvastatin showed increased microvessels in the peri-infarct region (n=4 in each group, $^{*}P<0.05$, $^{**}P<0.01$).

peri-infarct cortex and subventricular zone (Figure 2a). Although some BrdU-positive cells expressing DCX, a marker for migrating neuroblasts, could be detected in subventricular zone (Figure 2b), the percentage in total BrdU-positive cells (Figure 2g) and the number (Figure 2h) did not differ between the groups. Also, the number of DCX-positive cells was same in the both groups (Figure 2i). There were no BrdU-positive cells expressing DCX in the cerebral cortex. Unexpectedly, these data suggest that neurogenesis was not enhanced by fluvastatin.

Thus, we further examined whether angiogenesis was affected by fluvastatin. In the peri-infarct cortex and basal ganglia, BrdU-positive cells that were positive for CD31 as a marker of endothelial cells could be detected (Figure 2c,2d). The number of BrdU/CD31-double-positive cells was significantly increased in fluvastatin-treated rats (Figure 2j). The percentage of BrdU/CD31-double-positive cells in total BrdU-positive cells was also increased in fluvastatin-treated rats (Figure 2k). Consistently, microangiography using FITC-conjugated albumin[11] also showed that microvessels were significantly increased in fluvastatin-treated rats only in the peri-infarct cortex and basal ganglia, without destruction of the blood–brain (Figure 3a to 3h). Quantitative analysis showed that the length and area of microvessels were also increased in the peri-infarct region, but not in the contralateral cortex and contralateral basal ganglia, in rats treated with fluvastatin, at 3 months after stroke (Figure 3i,j).

Because recent reports showed that neurite outgrowth was observed in the peri-infarct region from 7 to 14 days after cerebral infarction,[16,17] we next examined the effect of fluvastatin on neurite outgrowth. Immunohistochemical staining showed that treatment with fluvastatin significantly increased the immunoreactivity of MAP1B, a marker of neurite outgrowth, in neurites[16,18] (Figure 4), although the number of MAP1B-positive cells was the same in both groups. These data implied that the fluvastatin might promote angiogenesis, resulting in improvement of the microcirculation, and neurite outgrowth.

One possible explanation for the enhanced angiogenesis and neurite outgrowth is a decrease in oxidative stress by fluvastatin. To assess oxidative stress, we evaluated superoxide production using dihydroethidium staining (Figure 5a to 5e). Superoxide anion was increased in the ischemic core as compared with the contralateral region at 2 weeks after MCA occlusion (Figure 5a,5c). However, rats treated with fluvastatin showed a significant reduction in superoxide anion especially in the ischemic core region, but not in the peri-infarct cortex and basal ganglia (Figure 5b,5d,5e).

Finally, we examined Aβ deposition in the thalamic nuclei, because previous reports showed that Aβ deposits in the

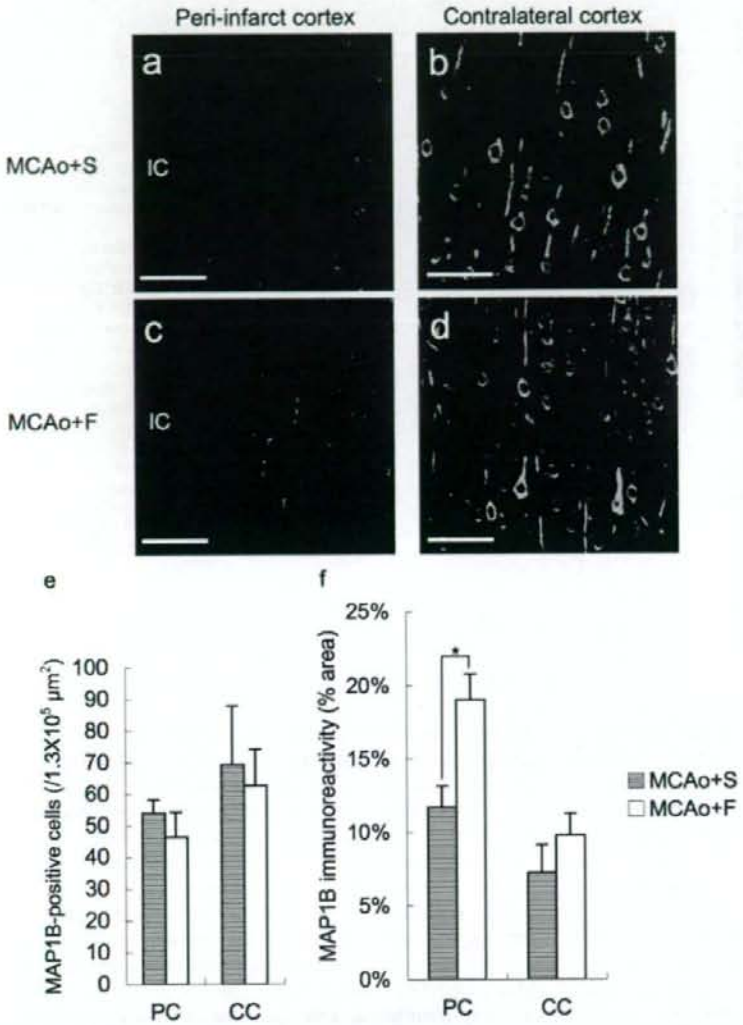

Figure 4. Typical images of immunohistochemical staining for MAP1B in peri-infarct cortex (a and c) and contralateral cortex (b and d) on day 14 (bar=100 μm). Although the number of MAP1B-positive cells was the same in both groups (e), immunoreactivity was higher in the peri-infarct region in fluvastatin-treated rats (f) (n=4 in each group, *$P<0.05$).

thalamic nuclei persisted as long as 9 months after focal cerebral ischemia.[12] Although immunohistochemical staining showed marked deposition of Aβ in the ventrolateral and ventromedial thalamic nuclei at 3 months after stroke, the area of Aβ deposits was significantly decreased in fluvastatin-treated rats (Figure 5f to 5h). In other regions, such as cortex or basal ganglia, there was no Aβ deposits in both groups as reported before.[12]

Discussion

Although several laboratories have shown that long-term pretreatment with a statin reduces infarct size in rodents,[19] no articles have reported the effects of delayed postischemic treatment with statins. The present study demonstrated that statin treatment beginning 7 days after ischemic stroke resulted in significant improvement of spatial learning at 8 weeks after stroke, without any change in the plasma cholesterol level and infarct size.

Fluvastatin-treated rats showed a significant increase of MAP1B in neurites in the peri-infarct region. Considering that MAP1B is especially prominent in extending neurites[20] and related to functional recovery after ischemic stroke,[17] one of the possible effects of fluvastatin is to enhance neurite outgrowth, "neuritogenesis," in the early stage of treatment. This speculation might be supported by the recent study demonstrating that neurite outgrowth is accelerated by pravastatin via inhibiting the activity of geranylgeranylated proteins such as RhoA.[21]

As BrdU/CD31-positive cells were increased 14 days after MCAo and microvessels were also increased in the peri-infarct region 100 days after MCAo, fluvastatin enhanced angiogenesis and resulted in improvement of microcirculation in the peri-infarct region. Although the relationship between the improved microcirculation and behavior is still unclear, a recent report demonstrated that the restoration of perfusion by collateral growth and new capillaries in the

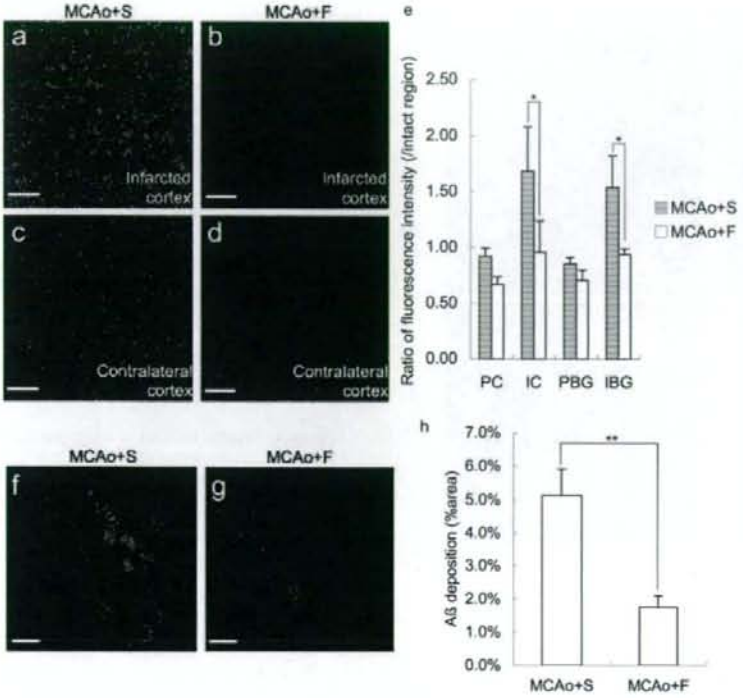

Figure 5. a through e, Superoxide anion detected by dihydroethidium staining on day 14. Red spots show the existence of superoxide anion. Fluorescence intensity was higher in the infarcted cortex (a) compared with the contralateral cortex (c). Fluvastatin-treated rats showed decreased fluorescence intensity in the infarcted cortex (b), although there was no difference in the peri-infarct cortex and basal ganglia (e) (n=4 in each group, $^{*}P<0.05$, bar=100 μm). Deposition of Aβ in thalamus on day 100 after middle cerebral artery occlusion. Although deposition of Aβ was observed in the thalamic nuclei (f and g), there was no deposition in other regions such as the cortex and basal ganglia. Quantitative analysis showed decreased Aβ deposition in fluvastatin-treated rats (h) (n=6 in each group, $^{**}P<0.01$, bar=200 μm).

ischemic border zone around a cortical infarct supported long-term functional recovery in rats.[22] Additionally, others reported that some patients who received tissue plasminogen activator therapy with no immediate clinical improvement despite early recanalization showed delayed clinical improvement.[23] From these viewpoints, it is likely that the improvement of microcirculation is an important factor for the functional recovery.

Of importance, fluvastatin reduced deposition of Aβ in the ventrolateral–ventromedial thalamic nuclei in the chronic stage of ischemic stroke, although rats subjected to focal cerebral ischemia develop deposition of Aβ in the ventroposterior lateral and ventroposterior medial nuclei for as long as 9 months.[12] This might be similar with precious reports showing that statins reduced the production of Aβ in Alzheimer disease.[24] The mechanism of the reduction of Aβ by fluvastatin should be further investigated.

Thus, the rats treated with fluvastatin showed enhancement of angiogenesis and neurite outgrowth in the peri-infarct cortex and reduced deposition of Aβ in the ventrolateral–ventromedial thalamic nuclei. Because those regions are important sites for spatial learning,[25,26] we speculate that the enhancement of functional recovery by fluvastatin might be dependent on those regions.

The other histological difference was the reduction of superoxide anion in the ischemic core in fluvastatin-treated rats. Because cerebral blood flow in the ischemic cortex remained to be reduced for 48 hours and restored to some extent 9 days after permanent MCAo,[27] we speculate that fluvastatin could reach the ischemic core and show the antioxidative effects. On the contrary, in the peri-infarct region, superoxide anion was not detected even in the control group and no effect of fluvastatin might be observed. This effect of statin is similar with the previous report showing that cerivastatin prevented the production of superoxide anion in the cerebral parenchyma in stroke-prone spontaneously hypertensive rats.[28] Also, fluvastatin is reported to possess antioxidative properties in other cells.[29,30]

The association of neurogenesis is also the center of interest, because previous reports showed an increase in neurogenesis after atorvastatin treatment beginning at 1 day after stroke.[5] However, we speculate that neurogenesis might not have contributed to the favorable outcome in the present study, because the volume of infarction was not decreased by fluvastatin, and the density of mature neurons (NeuN-positive cells) and proliferative immature neurons (BrdU/DCX-positive cells) was the same in both groups. From the viewpoints, the timing of treatment seems important for the enhancement of neurogenesis and the beginning of statin 7 days after MCAo might be too late to enhance neurogenesis.

The limitation of the present study is that there is no data demonstrating that fluvastatin crossed over the blood–brain barrier and acted on neurons directly. Blood–brain barrier permeability differs among statins and correlates in part with their respective lipophilicity.[31] Considering that pretreatment with pravastatin and rosuvastatin, whose lipophilicity is 0.84 and 0.33, respectively, shows significant effects on reducing infarction volume,[31] fluvastatin, whose lipophilicity is 1.27, might penetrate blood–brain barrier and have some direct effects on neurons. Otherwise, fluvastatin could penetrate the brain because of the disruption of blood–brain barrier after MCAo. One of other limitations in the present study is no

examination of the characteristics of BrdU positive-cells other than CD31, DCX, or NeuN. In addition, how these histological changes in fluvastatin-treated rats were mechanistically linked to improved outcome was not clarified. Further study is necessary to clarify these points.

Summary

Overall, delayed postischemic chronic fluvastatin treatment showed beneficial effects on the recovery of cognitive impairment after stroke by enhancement of neuritogenesis and of angiogenesis and a decrease in Aβ deposition and superoxide anion production. Further studies might show potential clinical utility to treat cognitive impairment in patients with ischemic stroke.

Acknowledgments

The authors thank Dr Masatsugu Horiuchi and Dr Masaru Iwai for their helpful advice on superoxide detection by dihydroethidium staining, and Dr Hiroshi Sato for assistance with MRI.

Sources of Funding

This work was partially supported by a Grant-in-Aid from the Organization for Pharmaceutical Safety and Research, a Grant-in-Aid from The Ministry of Public Health and Welfare, a Grant-in-Aid from Japan Promotion of Science, and a Grant-in-Aid from the Ministry of Education, Culture, Sports, Science, and Technology, of the Japanese Government.

Disclosures

Fluvastatin was donated from Novartis Pharma. Masataka Sata received Honoraria payment (modest) from Novartis Pharma. Ryuichi Morishita received honoraria payment (modest) and has an advisory board relationship to Novartis Pharma.

References

1. Sacks FM, Pfeffer MA, Moye LA, Rouleau JL, Rutherford JD, Cole TG, Brown L, Warnica JW, Arnold JM, Wun CC, Davis BR, Braunwald E. The effect of pravastatin on coronary events after myocardial infarction in patients with average cholesterol levels: cholesterol and recurrent events trial investigators. *N Engl J Med*. 1996;335:1001–1009.
2. Amarenco P, Tonkin AM. Statins for stroke prevention: disappointment and hope. *Circulation*. 2004;109:III44–49.
3. Moonis M, Kane K, Schwiderski U, Sandage BW, Fisher M. HMG-CoA reductase inhibitors improve acute ischemic stroke outcome. *Stroke*. 2005;36:1298–1300.
4. Chen J, Zhang C, Jiang H, Li Y, Zhang L, Robin A, Katakowski M, Lu M, Chopp M. Atorvastatin induction of VEGF and BDNF promotes brain plasticity after stroke in mice. *J Cereb Blood Flow Metab*. 2005;25:281–290.
5. Chen J, Zhang ZG, Li Y, Wang Y, Wang L, Jiang H, Zhang C, Lu M, Katakowski M, Feldkamp CS, Chopp M. Statins induce angiogenesis, neurogenesis, and synaptogenesis after stroke. *Ann Neurol*. 2003;53:743–751.
6. Zhang L, Zhang ZG, Ding GL, Jiang Q, Liu X, Meng H, Hozeska A, Zhang C, Li L, Morris D, Zhang RL, Lu M, Chopp M. Multitargeted effects of statin-enhanced thrombolytic therapy for stroke with recombinant human tissue-type plasminogen activator in the rat. *Circulation*. 2005;112:3486–3494.
7. Belayev L, Alonso OF, Busto R, Zhao W, Ginsberg MD. Middle cerebral artery occlusion in the rat by intraluminal suture: neurological and pathological evaluation of an improved model. *Stroke*. 1996;27:1616–1623.
8. Sata M, Nishimatsu H, Osuga J, Tanaka K, Ishizaka N, Ishibashi S, Hirata Y, Nagai R. Statins augment collateral growth in response to ischemia but they do not promote cancer and atherosclerosis. *Hypertension*. 2004;43:1214–1220.
9. Nakatomi H, Kuriu T, Okabe S, Yamamoto S, Hatano O, Kawahara N, Tamura A, Kirino T, Nakafuku M. Regeneration of hippocampal pyramidal neurons after ischemic brain injury by recruitment of endogenous neural progenitors. *Cell*. 2002;110:429–441.
10. Petullo D, Masonic K, Lincoln C, Wibberley L, Teliska M, Yao DL. Model development and behavioral assessment of focal cerebral ischemia in rats. *Life Sci*. 1999;64:1099–1108.
11. Cavaglia M, Dombrowski SM, Drazba J, Vasanji A, Bokesch PM, Janigro D. Regional variation in brain capillary density and vascular response to ischemia. *Brain Res*. 2001;910:81–93.
12. van Groen T, Puurunen K, Maki HM, Sivenius J, Jolkkonen J. Transformation of diffuse beta-amyloid precursor protein and beta-amyloid deposits to plaques in the thalamus after transient occlusion of the middle cerebral artery in rats. *Stroke*. 2005;36:1551–1556.
13. Iwai M, Liu HW, Chen R, Ide A, Okamoto S, Hata R, Sakanaka M, Shiuchi T, Horiuchi M. Possible inhibition of focal cerebral ischemia by angiotensin II type 2 receptor stimulation. *Circulation*. 2004;110:843–848.
14. Robinson RG. Differential behavioral and biochemical effects of right and left hemispheric cerebral infarction in the rat. *Science*. 1979;205:707–710.
15. DeVries AC, Nelson RJ, Traystman RJ, Hurn PD. Cognitive and behavioral assessment in experimental stroke research: Will it prove useful? *Neurosci Biobehav Rev*. 2001;25:325–342.
16. Badan I, Platt D, Kessler C, Popa-Wagner A. Temporal dynamics of degenerative and regenerative events associated with cerebral ischemia in aged rats. *Gerontology*. 2003;49:356–365.
17. Badan I, Dinca I, Buchhold B, Suofu Y, Walker L, Gratz M, Platt D, Kessler CH, Popa-Wagner A. Accelerated accumulation of n- and c-terminal beta app fragments and delayed recovery of microtubule-associated protein 1b expression following stroke in aged rats. *Eur J Neurosci*. 2004;19:2270–2280.
18. Schabitz WR, Berger C, Kollmar R, Seitz M, Tanay E, Kiessling M, Schwab S, Sommer C. Effect of brain-derived neurotrophic factor treatment and forced arm use on functional motor recovery after small cortical ischemia. *Stroke*. 2004;35:992–997.
19. Endres M, Laufs U, Liao JK, Moskowitz MA. Targeting enos for stroke protection. *Trends Neurosci*. 2004;27:283–289.
20. Gonzalez-Billault C, Avila J, Caceres A. Evidence for the role of map1b in axon formation. *Mol Biol Cell*. 2001;12:2087–2098.
21. Pooler AM, Xi SC, Wurtman RJ. The 3-hydroxy-3-methylglutaryl co-enzyme a reductase inhibitor pravastatin enhances neurite outgrowth in hippocampal neurons. *J Neurochem*. 2006;97:716–723.
22. Wei L, Erinjeri JP, Rovainen CM, Woolsey TA. Collateral growth and angiogenesis around cortical stroke. *Stroke*. 2001;32:2179–2184.
23. Alexandrov AV, Hall CE, Labiche LA, Wojner AW, Grotta JC. Ischemic stunning of the brain: Early recanalization without immediate clinical improvement in acute ischemic stroke. *Stroke*. 2004;35:449–452.
24. Fassbender K, Simons M, Bergmann C, Stroick M, Lutjohann D, Keller P, Runz H, Kuhl S, Bertsch T, von Bergmann K, Hennerici M, Beyreuther K, Hartmann T. Simvastatin strongly reduces levels of Alzheimer's disease beta -amyloid peptides Abeta 42 and Abeta 40 in vitro and in vivo. *Proc Natl Acad Sci U S A*. 2001;98:5856–5861.
25. Casu MA, Wong TP, De Koninck Y, Ribeiro-da-Silva A, Cuello AC. Aging causes a preferential loss of cholinergic innervation of characterized neocortical pyramidal neurons. *Cereb Cortex*. 2002;12:329–337.
26. Jeljeli M, Strazielle C, Caston J, Lalonde R. Effects of ventrolateral-ventromedial thalamic lesions on motor coordination and spatial orientation in rats. *Neurosci Res*. 2003;47:309–316.
27. Rudin M, Baumann D, Ekatodramis D, Stirnimann R, McAllister KH, Sauter A. MRI analysis of the changes in apparent water diffusion coefficient, t(2) relaxation time, and cerebral blood flow and volume in the temporal evolution of cerebral infarction following permanent middle cerebral artery occlusion in rats. *Exp Neurol*. 2001;169:56–63.
28. Kawashima S, Yamashita T, Miwa Y, Ozaki M, Namiki M, Hirase T, Inoue N, Hirata K, Yokoyama M. HMG-CoA reductase inhibitor has protective effects against stroke events in stroke-prone spontaneously hypertensive rats. *Stroke*. 2003;34:157–163.
29. Sumi D, Hayashi T, Thakur NK, Jayachandran M, Asai Y, Kano H, Matsui H, Iguchi A. A HMG-CoA reductase inhibitor possesses a potent anti-atherosclerotic effect other than serum lipid lowering effects–the relevance of endothelial nitric oxide synthase and superoxide anion scavenging action. *Atherosclerosis*. 2001;155:347–357.
30. Morita H, Saito Y, Ohashi N, Yoshikawa M, Katoh M, Ashida T, Kurihara H, Nakamura T, Kurabayashi M, Nagai R. Fluvastatin ameliorates the hyperhomocysteinemia-induced endothelial dysfunction: The antioxidative properties of fluvastatin. *Circ J*. 2005;69:475–480.
31. Endres M. Statins and stroke. *J Cereb Blood Flow Metab*. 2005;25:1093–1110.

特集論文／分子イメージング時代の画像解析・データ解析の新しい視点

マイクロ SPECT を用いた小動物イメージングの定量的機能評価
Quantitative Functional Imaging of Small Animals Using MicroSPECT

銭谷　勉*
Tsutomu ZENIYA

要　旨

創薬や新規治療法の評価を目的とした前臨床研究において，小動物モデルを用いた in vivo イメージングは不可欠である．その中でも PET や SPECT などの高感度トレーサ技術である核医学的手法は生体内の生理機能を定量評価できるため大きな役割を果たしている．本論文では，小動物イメージングにおける定量的機能評価の意義および応用領域について言及した上で，マイクロ SPECT における動態解析および画像再構成の定量性について概論する．また，マイクロ SPECT を利用した定量的機能評価の例を紹介する．
キーワード：小動物，定量的機能評価，SPECT，ピンホールコリメータ，画像再構成

In vivo imaging of small laboratory animals facilitates objective assessment of pharmaceutical development and regenerative therapy in pre-clinical studies. Radionuclide imaging such as PET or SPECT is especially important because it allows to quantitatively assess physiological functions due to high sensitive tracing technique. This paper describes the significances and applications of quantitative functional assessment in small animal imaging, and then discusses quantitation about kinetic analysis and image reconstruction in microSPECT. Finally, it introduces quantitative functional imaging studies using microSPECT.
Key words: Small animal, Quantitative functional imaging, SPECT, Pinhole collimator, Image reconstruction
Med Imag Tech **26**(1): 14-20, 2008

1. はじめに

創薬や新規治療法を目的とした前臨床研究において，ラットやマウスなどの小動物モデルを用いた in vivo イメージングは不可欠である．また，近年の分子イメージング分野の発展に伴い，小動物専用の X 線 CT（Computed Tomography），MRI（Magnetic Resonance Imaging），PET（Positron Emission Tomography），SPECT（Single Photon Emission CT）および光イメージングなどの装置が盛んに開発されている．その中でも，PET や SPECT などの放射性同位元素をトレーサとして用いる核医学検査手法は，高い感度を有し，トレーサの集積の対して正確に比例した信号強度を提示するため，病態生理や病態生化学的な変化を定量に評価することが可能であるため重要な役割を果たしている．

PET 装置は高い感度を有するが，高解像度の小動物用 PET 装置でもその空間解像度は 1 mm を超えておらず〔1〕，小病変の画像化に不十分である．PET は放射線同位元素から放出される陽電子が電子と結合する際に反対方向に放出される 2 本の消滅放射線をリング状の検出器で同時計測することで，放射線同位元素の存在する位置を推定する．陽電子が静止するまでの距離を陽電子の飛程と呼ぶが，核種によっては飛程が装置の空間解像度よりも大きく，解像度を悪化させる．たとえば，^{15}O の場合，陽電子のエネルギーが高く，陽電子が消滅するまでに水中で平均 2.5 mm 移動する．また，PET 核種は半減期が短いため，小動物実験において，同一の個体の

* 国立循環器病センター研究所先進医工学センター放射線医学部〔〒 565-8565 大阪府吹田市藤白台 5-7-1〕：National Cardiovascular Center Research Institute.
e-mail: zeniya@ri.ncvc.go.jp
論文受付：2007 年 12 月 25 日
最終稿受付：2008 年 1 月 7 日

繰り返し撮像が行いやすいという利点である反面，サイクロトロンや放射性薬剤合成装置などの大掛かりな設備を必要とする．一方，SPECT装置は放射線同位元素から放出されるガンマ線の飛来方向を特定するためのコリメータを必要とするため，コリメータを必要としないPETに比べ感度が劣るのは避けられないが，コリメータの工夫次第ではPETよりも高い空間解像度が得られる．ピンホールコリメータは対象物がコリメータに近いほど感度および空間解像度を高くできるので（**Fig. 1**），小動物イメージングに適しており，1 mm以下の解像度が比較的容易に実現できる〔2, 3〕．ほとんどの小動物用SPECT装置（マイクロSPECT）ではこのピンホールコリメータを利用している．感度が低いという問題は，複数のピンホールを利用することで克服する試みが行われている〔4～6〕．また，**Table 1**に示されているようにSPECT検査で使用される放射性核種は半減期が長いため，PETでは観測できない，長時間における薬剤の動態を観察したいという場合に適している．そして，何よりも放射性薬剤を他施設から入手できるため，安価で手軽に検査が実施できるという大きな利点がある．

Geometric resolution (R_g)

$$R_g = (a+b)\frac{d_e}{a}$$

d_e: effective pinhole diameter

System resolution (R_o)

$$R_o = \sqrt{R_g^2 + \frac{b}{a}R_i^2}$$

R_i: intrinsic detector resolution

Resolution	$\propto d_e \times (a+b)/a$
Sensitivity	$\propto d_e^2/b^2$

Fig. 1 Physics of pinhole SPECT. Spatial resolution and sensitivity can be improved by positioning a collimator closer to an object.

従来のピンホールSPECTは，体軸方向に画像が歪み，視野内の解像度が不均一になるという問題があったため，定量評価が困難であった．著者らは，この原因をデータの不完全性によるものと仮説をたて，撮像軌道をラドン変換の完全性を満たすように設計し，立体的な画像再構成理論を導入することで，歪みのない視野全体で均一な解像度を有する3次元画像を得ることに成功した〔7〕．その結果，ピンホールSPECTにおいても小動物PET同様に定量評価が可能になった．しかしながら，PETやSPECTが得意とする，定量的な機能評価をマイクロSPECTで行う試みは，それほど広くなされていない．

本論文では，小動物イメージングにおける定量的機能評価に必要とされる著者らの物理工学的な最近の進歩について述べる．最初に，小動物イメージングの定量的機能評価の意義および応用領域について言及した上で，マイクロSPECTにおける動態解析および画像再構成の定量性ついて概論する．最後に，著者らが開発したマイクロSPECT装置を利用した定量的機能評価の例を紹介する．

2. 小動物イメージングにおける定量的機能評価の意義と応用領域

通常，遺伝子改変や病態モデル動物はマウスやラットなどの小動物に対して行われており，生きたまま，小動物内の分子をイメージングする技術は非常に重要である．とくに，ヒトから実

Table 1 Representative radionuclides used in SPECT study.

Isotope	Energy	Half life	Tracer	Application
^{99m}Tc	140 keV	6.01 hr	MDP/HMDP	bone scan
			MIBI	myocardial perfusion
			tetrofosmin	myocardial perfusion
			TRODAT	dopamine transporter
^{201}Tl	70 keV	72.9 hr	TlCl	myocardial perfusion
^{123}I	159 keV	13.3 hr	BMIPP	beta-oxidation
			MIBG	sympathetic
			β-CIT	dopamine transporter
			Iomazenil	benzodiazepine receptor
^{131}I	364 keV	8.04 day		thyroid
^{67}Ga	93, 185, 300 keV	3.26 day	citrate	tumor

験小動物まで同じ手技で定量的機能評価が可能な核医学イメージング技術は，血流などの生理的機能から種々の受容体，遺伝子発現，ペプチド・タンパクなどの疾患関連物質の体内動態までを観察できるため，創薬の迅速化・低コスト化や，テーラーメード医療，遺伝子治療，再生医療などに代表される新しい病気の診断・治療法の開発に大きく貢献するといわれている．

創薬においては，治療化合物の探索から体内吸収・体内動態の評価，臨床試験早期に必要な毒性と薬効評価，投与量の最適化などの分野においての利用が開始されている．再生医療分野においても，多くの局面で本質的な情報を提示し，有効な治療法の確立に向けて重要な役割を果たすことは明らかである．たとえば，心筋梗塞部位での血管新生治療，細胞移植治療では，細胞の定着や血管の発達などの形態的な再生だけでなく，生体の一部の組織として機能評価を行うことが必要である．定着した細胞および組織の血流がどの程度回復し，種々の生理的な負荷などによって本来持つべき反応力（血流の自動調節能と血管反応性，代謝の制御，神経連絡過程など）をどの程度有し，必要な生体フィードバックを可視化できることが望ましい．これらの分野の基盤技術を整備するためには，疾患の本質を理解すること，そのための基礎，前臨床，および臨床研究を並行して実施すること，また，本質的な治療実施のための各種基盤技術を有していることが不可欠である．

3. マイクロ SPECT による定量的機能評価の問題点

SPECT データから，血流量，結合能などの定量的な生理パラメータを得るためには，コンパートメントモデル解析やグラフ解析など，トレーサの動態解析を行う必要がある〔8〕．このとき，入力関数と呼ばれる動脈中の放射能濃度の投与時からの時間変化が必要となる．ヒトの場合，通常，腕の動脈に穿刺し，撮像中にマニュアルで頻回採血やポンプを用いた連続採血を行って入力関数を得る〔9〕．ラットやマウスの血液量は，ヒトに比べて少量のため，採血量が多くなると貧血を起こし，生理状態も大きく変化する．そのため，最低限の採血量に抑える必要があり，動脈と静脈を短絡させる arteriovenous（AV）シャント術を施し，そこから入力関数を得る方法が提案されている．

心筋機能の定量では，撮像された左心室から入力関数を得る方法が用いられる．しかし，これらの方法で得られる入力関数はあくまでも全血の放射能濃度であり，放射性薬剤が体内で代謝される場合，代謝産物の定量も行う必要もある．微量の血液中の代謝産物の定量は非常に困難である．このため，あらかじめ複数の同一動物で測定した平均入力関数を用いる方法や，入力関数の代わりにリファレンス領域を用いる方法〔10〕がしばしば使われる．

得られたパラメータを解釈する際には，ヒトとの違いを考慮する必要がある．代謝速度はヒトと小動物では大きく異なる．通常，小動物の撮像は麻酔下で行われるが，麻酔の影響も無視できない．著者らは覚醒下に適したラット専用のホルダーを作製し，1 週間の馴化を行うことによって，覚醒下でのラット心筋血流定量測定および血管反応性の評価を可能にした．

4. マイクロ SPECT 画像再構成における定量性

前述のようなトレーサの動態解析を行う場合，SPECT 画像の定量性が確保されていることが前提である．マイクロ SPECT 画像再構成においても，定量性を劣化させる要因を十分に考慮する必要がある．

1）部分容積効果

核医学装置は，定量性が高いとしばしばいわれるが，部分容積効果（小さい対象物を空間解像度の悪い装置で撮像したとき発生する測定値の過小評価）は大きく定量性に影響する．とくに，小動物の場合サイズがヒトより小さいため，相応の高い空間解像度が要求される．たとえば，臨床で利用されている PET 装置は 5 mm 程度の空間解像度を持つが，この装置で得られた画像と同等の解像度でラットを撮像したければ 0.6 mm，マウスでは 0.4 mm の空間解像度が要求される〔1〕．実際の小動物用 PET の空間解像度は 1 ～ 2 mm 程度であるため，部分容積効果は小動物 PET ではヒトよりも大きな問題となる．これに対して，小動物用のピンホール SPECT では数百 μm の空間解像度を実現できるため，部分容積効果を抑制できる点で優位である．しかしなが

ら，部分容積効果の定量性に与える影響は少なくないため，定量する際は十分に考慮する必要がある．コリメータ開口補正技術〔11〕などを用いて解像度を改善するのも1つの方策である．

2）吸収・散乱

SPECT で定量性を劣化させる大きな要因として，被写体内でのガンマ線の吸収および散乱がある．一般的な臨床脳 SPECT 検査では，60 ～ 80% の光子が体内での吸収を受け，30 ～ 40% の光子が散乱によって偽りの信号を与える．これらの影響を補正しなければ定量評価は難しい．飯田らは，実用的な手法によって吸収・散乱の影響を高い精度で補正することに成功し，SPECT でも PET 同様の定量評価を可能にした〔12〕．しかしながら，体内での吸収・散乱の影響は被写体の大きさに依存することを考えると，小動物ではヒトの場合に比べてそれほど大きくないと考えられる．Wang らはマウスにおける吸収・散乱の影響を，シミュレーションおよびファントム実験にて評価した．吸収も散乱も補正しない場合，15% 過小評価し，吸収補正のみ行った場合，9% 過大評価する．吸収と散乱の両方を補正して誤差は3%以下にできると報告している〔13〕．Deloar らは散乱線の影響に加え，ピンホールコリメータを突き抜けるガンマ線の影響も考慮する必要があることをシミュレーションによって示している〔14〕．この突き抜けガンマ線の影響はピンホール形状を knife-edge 型に代えて，keel-edge（channel-edge とも呼ぶ）型を使用することで抑制することができる〔15〕．

3）データの完全性

ピンホールコリメータを用いた SPECT 装置は原理上，3 次元収集を行っているが，コーンビーム型の 3 次元画像再構成法が必要となる．ピンポール SPECT において単一の円軌道でデータを収集した場合，体軸方向に画像が歪み，空間解像度が不均一となるため，定量解析は困難である．画像再構成法を解析的手法の FBP（Filtered Back-Projection）に代えて，OSEM（Ordered Subsets Expectation Maximization）などの統計学に基づいた逐次近似画像再構成法を使用することによって改善されるが，視野周辺では依然として解像度の劣化は残っている〔16〕．最近の研究で，著者らはこの原因をデータの不完全性に起因するものと仮説をたて，撮像軌道をラドン変換の完全性を満たすような複数回転軸軌道とし，これに立体的画像再構成理論を導入することで，視野内で均一な高解像度を得ることに成功した（**Fig. 2**）〔7〕．Metzler らはヘリカル軌道で完全データ収集を実現している〔17〕．従来は定性的な評価のみに利用されてきた高解像度撮像法のピンホール SPECT だが，この問題の解決によって PET 同様に定量解析が可能になった．

4）トランケーション

ピンホールコリメータは対象物がコリメータに近いほど感度および解像度を高くできるのが特長であるが，極端に近づけるとトランケーション（データの欠損）が生じ，再構成画像のカウントは過大評価され，定量評価の妨げとなる．通常は被写体が視野から外れないように，被写

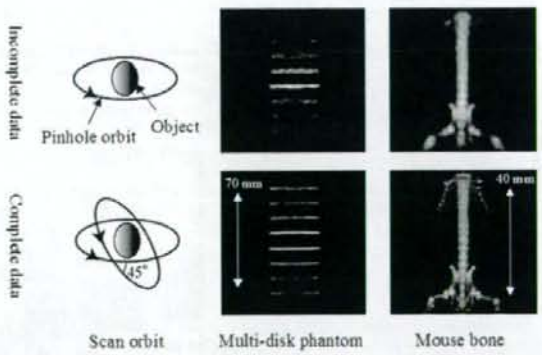

Fig. 2 Comparison between conventional acquisition and complete data acquisition in multi-disk phantom study and mouse bone scan with ^{99m}Tc. Data acquired by conventional single circular orbit are incomplete. Complete data are acquired by two-circular orbit. Complete data improve axial blurring and non-uniform spatial resolution in pinhole SPECT.

体からコリメータをある程度離して撮像する．ただし，これは解像度と感度を妥協することになる．著者らは，Defrise らが 2 次元 X 線 CT を対象として提案した理論〔18〕を基に，ピンホール SPECT でトランケーションを許す 3 次元画像再構成法 TC-OSEM（Truncation Compensated OSEM）を開発した〔19〕．本画像再構成理論では，**Fig. 3** に示すように収集データに被写体外のゼロ（既知）領域が含まれること，画像再構成マトリクスは被写体が完全に含まれるように十分に大きく設定することの 2 つの条件の下，OSEM などの逐次近似画像再構成法によって視野内は正確な値に収束する．本手法により，トランケーションがあっても定量性が確保される（**Fig. 4**）．

5. マイクロ SPECT を用いた定量的機能評価の例

1）ラット心筋血流量・血管反応性

近年高血圧や高脂血症などの循環器疾患に関与する遺伝子が明らかになってきており，疾患発現に先行する病態生理の把握が重要になる．このとき，安静時のみの組織血流量や基質代謝量に加えて，種々の生理的・薬理的な賦活に対する反応性，たとえば血管反応性や代謝自動調節能などが指標になると考えられている．

著者らは，小動物でこのような生理機能の定量評価を目的として，小型高解像度ピクセル型 NaI シンチレータとピンホールコリメータを組み合わせた検出器〔20〕を 4 台搭載した小動物専用高解像度 SPECT 装置を開発した（**Fig. 5**）．

本装置を用いて，覚醒下での健常ラットの心筋血流量および血管反応性を評価した．ラットは **Fig. 6** のように装置にセットされた．8 匹のラットを用いて ^{201}Tl を 36 分間隔で分割投与し，4 匹は安静時と安静時，残りの 4 匹は安静時と血管拡張時の心筋血流量を測定した．血管拡張時には血管拡張薬アデノシン A2A アゴニスト CGS21680 を 2 回目の ^{201}Tl 投与の 6 分前に投与した．ピンホール用 3D-OSEM で画像再構成して得られた一連の時系列画像データに対して 2 コンパートメントモデル〔21〕を適用した．**Fig. 7** は本実験で得られた心筋 SPECT 画像であるが，非常に鮮明な画像が得られた．入力関数は，別実験で 10 匹のラットの頻回採血から作成した標準入力関数を用いた．実験の結果，安静時と安静時の検査では血流値に変化はなく，安静時と負荷時の検査では血管拡張薬の量に依存して，血流上昇が認められた（**Fig. 8**）．本マイクロ SPECT システムで得られたデータを動態解析することで，小動物の心筋血流量および血管反応性を 1 回の検査で定量的に評価可能である．

2）マウス脳血流量

局所脳血流量は脳梗塞の治療効果を評価する

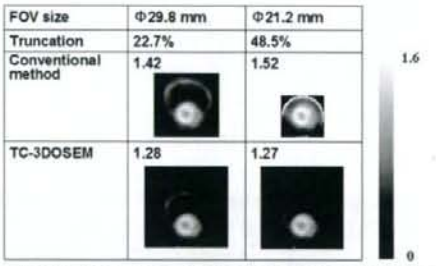

Fig. 4 Reconstructed images and myocardial counts obtained by conventional method and TC-3DOSEM. We artificially generated data with the different amount of truncation from rat experimental data. TC-3DOSEM method eliminates overestimation and provides quantitative image in independence of the amount of truncation.

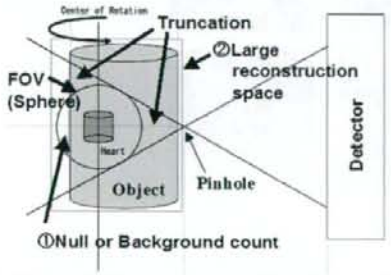

Fig. 3 Schematic diagram to show conditions for truncation compensated reconstruction in 3D pinhole SPECT.

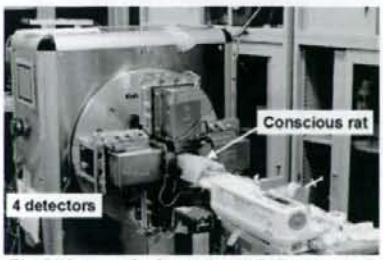

Fig. 5 Photograph of our microSPECT system and rat cardiac imaging study.

指標の1つである．6匹の脳梗塞モデルマウスを準備し，その中の3匹に対して骨髄単核球細胞を移植(治療)した．未治療群3匹と治療群3匹において，ピンホールSPECTと^{123}I-iodoamphetamine (IMP) を用いた脳組織血流定量の妥当性および移植治療効果を評価した．臨床用 SPECT 装置 (GCA-7200A, Toshiba) にピンホールコリメータを装着し，IMP 投与約10分後に摘出脳を回転ステージに載せ，各1時間 SPECT 撮像した．ピンホール用3D-OSEMで再構成して得られた画像に2コンパートメントモデル〔22〕を適用して，空間解像度 0.9 mm の3次元脳組織血流分布像を得た (**Fig. 9**)．入力関数は別実験で5匹のマウスの頻回採血によって得られた標準入力関数を利用し，分配定数は 45 ml/ml〔23〕を採用した．また，SPECT 撮像の前に MRI で T2 強調画像を得て位置合わせを行い，梗塞領域を特定した (**Fig. 9**)．得られた局所脳血流量は，正常側で 1.09 ± 0.21 ml/g/min であり，既報のノーマルマウスを 14C とオートラジオグラフィで測定した結果〔24〕の範囲であった．一方，梗塞巣で 0.76 ± 0.18 ml/g/min であり，有意に血流低下がみられた．また，未治療群と治療群の比較では，治療群で脳血流量の改善効果がみられた．ピンホール SPECT でマウス脳梗塞モデルを用いた病態の定量評価が可能である．今後，同一マウスによる in vivo 繰り返し撮像を予定している．また，^{123}I標識技術はペプチドやタンパクのイメージングを可能とし，マイクロ PET を補う技術になりうることが認められる．

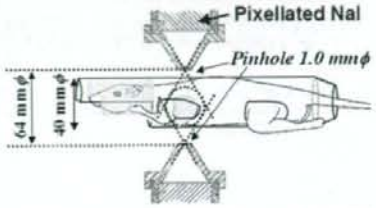

Fig. 6 Imaging geometry. Rat was set in a dedicated holder for conscious condition.

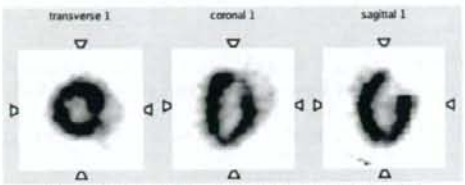

Fig. 7 Representative rat cardiac images obtained by our microSPECT and ^{201}Tl.

6. まとめ

創薬や治療法評価などの前臨床研究における小動物イメージングの定量的機能評価は重要な役割を担っている．高解像度を有するマイクロ SPECT 装置は最近の物理工学的な進歩によって小動物 PET 同様に定量解析が可能になったことと，検査の簡便さも手伝って今後広く普及するものと考えられる．

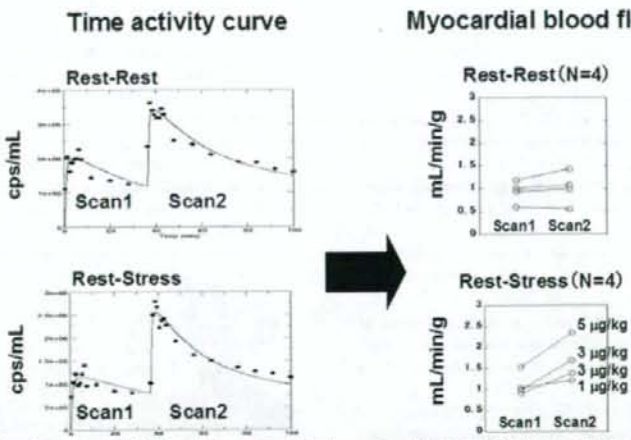

Fig. 8 Quantitaion of rat myocardial blood flow using data from microSPECT. Left: Representative time activity curves in rest-rest and rest-stress studies. Right: Myocardial blood flows calculated by two-compartment model. Coronary flow reserves were assessed in rest-stress studies.

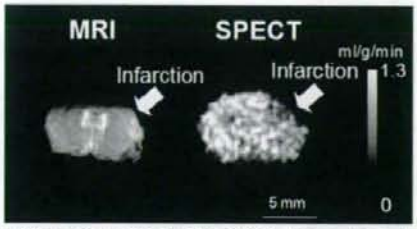

Fig. 9 Co-registrated MR and SPECT images of cerebral infraction model mouse. Left: T2 weighted image obtained by MRI. Right: Quantitative cerebral blood flow image obtained by pinhole SPECT and ^{123}I-IMP.

謝　辞

本研究の一部は，独立行政法人科学技術振興機構課題番号1702，および厚生労働科学研究費補助金「こころの健康科学研究」により実施された．

文　献

[1] Larobina M, Brunetti A, Salvatore M : Small animal PET: a review of commercially available imaging systems. Curr Med Imag Rev **2**: 187-192, 2006

[2] Miekle SR, Kench P, Kassiou M et al : Small animal SPECT and its place in the matrix of molecular imaging technologies. Phys Med Biol **50**: R45-R61, 2005

[3] 銭谷　勉，渡部浩司，工藤博幸，他：完全データを利用したピンホール SPECT．Med Imag Tech **23**: 9-16, 2005

[4] Liu Z, Kastis GA, Stevenson GD et al: Quantitative analysis of acute myocardial infarct in rat hearts with ischemia-reperfusion using a high-resolution stationary SPECT system. J Nucl Med **43**: 933-939, 2002

[5] Schramm NU, Ebel G, Engeland U et al: High-resolution SPECT using multipinhole collimation. IEEE Trans Nucl Sci **50**: 315-320, 2003

[6] Beekman FJ, van der Have F, Vastenhouw B et al: U-SPECT-I: a novel system for submillimeter-resolution tomography with radiolabelled molecules in mice. J Nucl Med **46**: 1194-1200, 2005

[7] Zeniya T, Watabe H, Aoi T et al: A new reconstruction strategy for image improvement in pinhole SPECT. Eur J Nucl Med Mol Imaging **31**: 1166-1172, 2004

[8] Watabe H, Ikoma Y, Kimura Y et al: PET kinetic analysis-compartmental model. Ann Nucl Med **20**: 583-589, 2006

[9] Kudomi N, Choi E, Yamamoto S et al: Development of a GSO detector assembly for a continuous blood sampling system. IEEE Trans Nucl Sci **50**: 70-73, 2003

[10] Acton PD, Choi S-R, Plössl K et al: Quantification of dopamine transporters in the mouse brain using ultra-high resolution single-photon emission tomography. Eur J Nucl Med **29**: 691-698, 2002

[11] Sohlberg A, Watabe H, Zeniya T et al: Comparison of multi-ray and point-spread function based resolution recovery methods in pinhole SPECT reconstruction. Nucl Med Commun **27**: 823-827, 2006

[12] 飯田秀博，渡部浩司，赤松哲哉，他：SPECTを使った脳機能画像の定量化と標準化．脳神経外科ジャーナル **16**: 742-752, 2007

[13] Wang Y, Du Y, Mok SP et al: Towards quantitative high-resolution pinhole SPECT imaging. [Abstract] J Nucl Med **45**(suppl 2): 110, 2005

[14] Deloar H, Watabe H, Aoi T et al: Evaluation of penetration and scattering components in conventional pinhole SPECT: phantom studies using Monte Carlo simulation. Phys Med Biol **48**: 995-1008, 2003

[15] van der Have F, Beekman FJ: Penetration and scatter in channel micro-pinholes for SPECT: a Monte Carlo investigation. 2004 IEEE Nuclear Science Symposium Conference Record **4**: 2575 - 2578, 2004

[16] Vanhove C, Defrise M, Franken PR et al: Interest of the ordered subsets expectation maximization (OS-EM) algorithm in pinhole single-photon emission tomography reconstruction: a phantom study. Eur J Nucl Med **27**: 140-146, 2000

[17] Metzler SD, Greer KL, Jaszczak RJ: Helical pinhole SPECT for small-animal imaging: a method for addressing sampling completeness. IEEE Trans Nucl Sci **50**: 1575-1583, 2003

[18] Defrise M, Noo F, Clackdoyle R et al: Truncated Hilbert transform and image reconstruction from limited tomographic data. Inverse Probl **22**: 1037-1053, 2006

[19] Zeniya T, Watabe H, Sohlberg A et al: 3D-OSEM reconstruction from truncated data in pinhole SPECT. 2007 IEEE Nuclear Science Symposium Conference Record: 4205-4207, 2007

[20] Zeniya T, Watabe H, Aoi T et al: Use of a compact pixellated gamma camera for small animal pinhole SPECT imaging. Ann Nucl Med **20**: 409-416, 2006

[21] Iida H, Eberl S: Quantitative assessment of regional myocardial blood flow with thallium-201 and SPECT. J Nucl Cardiol **5**: 313-331, 1998

[22] Iida H, Itoh H, Nakazawa M et al: Quantitative mapping of regional cerebral blood flow using iodine-123-IMP and SPECT. J Nucl Med **35**: 2019-2030, 1994

[23] Iida H, Akutsu T, Endo K et al: A multicenter validation of regional cerebral blood flow quantitation using [^{123}I]iodoamphetamine and single photon emission computed tomography. J Cereb Blood Flow Metab **16**: 781-793, 1996

[24] Maeda K, Mies G, Oláh L et al: Quantitative measurement of local cerebral blood flow in the anesthetized mouse using intraperitoneal [14C]iodoantipyrine injection and final arterial heart blood sampling. J Cereb Blood Flow Metab **20**: 10-14, 2000

銭谷　勉（ぜにや　つとむ）

1991年山形大学工学部情報工学科卒業．1993 年山形大学大学院工学研究科情報工学専攻修士課程修了．同年㈱日立メディコ入社．2002 年山形大学大学院理工学研究科システム情報工学専攻博士後期課程修了．2001–2002 年日本学術振興会特別研究員．現在，国立循環器病センター研究所先進医工学センター放射線医学部特任研究員．博士（工学）．小動物 SPECT，画像再構成法の研究開発に従事．1998 年日本医用画像工学会論文賞．2005 年日本核医学会研究奨励賞．

ELSEVIER

Nutrition 23 (2007) 81–86

NUTRITION

www.elsevier.com/locate/nut

Basic nutritional investigation

Kurozu moromimatsu inhibits tumor growth of Lovo cells in a mouse model in vivo

Naoto Fukuyama, M.D., Ph.D.[a,*], Shio Jujo[a], Isao Ito, M.D., Ph.D.[b], Toru Shizuma, M.D., Ph.D.[a], Kazunori Myojin, M.D., Ph.D.[c], Kazuo Ishiwata, Ph.D.[a], Masanobu Nagano, Ph.D.[d], Hiroe Nakazawa, M.D., Ph.D.[a], and Hidezo Mori, M.D., Ph.D.[e]

[a] *Department of Physiology, Tokai University, School of Medicine, Isehara, Kanagawa, Japan*
[b] *Department of Surgery, Tokai University, School of Medicine, Isehara, Kanagawa, Japan*
[c] *Department of Radiology, Tokai University, School of Medicine, Isehara, Kanagawa, Japan*
[d] *Sakamoto Jozo Inc., Kagoshima, Kagoshima, Japan*
[e] *Department of Cardiac Physiology, National Cardiovascular Center, Suita, Osaka, Japan*

Manuscript received June 2, 2006; accepted October 12, 2006.

Abstract

Objective: In Japan, rice vinegar that has been matured and fermented for years in earthenware jars is considered a health food with anticolon cancer action. It is divided into the liquid component (Kurozu) and the sediment (Kurozu moromimatsu), which contains large amounts of organic materials and minerals. The effect of Kurozu moromimatsu (Kurozu-M) on cancer has not yet been examined. In this study, we examined the activity of Kurozu-M on colon cancer and investigated the mechanisms involved, focusing on active oxygen generation, apoptosis, and metalloproteinases (MMPs).

Methods: We used Lovo cells transplanted into nude mice as an experimental model. We measured the tumor volume and MMP levels and conducted hematoxylin-eosin staining (for polymorphonuclear leukocytes), terminal deoxynucleotidyl transferase-mediated dUTP nick end-labeling staining (for apoptosis), and immunostaining for nitrotyrosine (a marker of active oxygen generation) in control, Kurozu-treated, and Kurozu-M—treated groups.

Results: The tumor volume was the same in the control group (231 ± 36 mm^3) and Kurozu group (238 ± 52 mm^3), but was significantly reduced in the Kurozu-M group (152 ± 28 mm^3, $P < 0.001$ versus control). Apoptosis of tumor cells and accumulation of polymorphonuclear leukocytes were not observed. Nitrotyrosine production, total MMP levels, and MMP activation were significantly reduced in the Kurozu-M group.

Conclusion: The administration of Kurozu-M prolonged the lifespan of cancer cell–transplanted mice, inhibited tumor progression, and reduced nitrotyrosine production and MMP activation, but did not induce apoptosis.

Keywords: Kurozu; Kurozu moromimatsu; Lovo cell; Colon cancer

This work was supported by grants from Tokai University School of Medicine Research Aid in 2004, 2005, and 2006; the research and study program of Tokai University Educational System General Research Organization; the Kanagawa Nanbyou Foundation in 2004; Grants-in-Aid for Scientific Research in 2003 (grant 15659285), 2005 (grant 17659375), and 2006 (grant 18390336) from the Ministry of Education, Science and Culture, Japan; Health and Labour Sciences Research Grants for Research on Human Genome, Tissue Engineering Food Biotechnology in 2003 (grant H15-saisei-003); Health and Labour Sciences Research Grants for Comprehensive Research on Cardiovascular Diseases in 2004 (grant H16-jyunkannki[seishuu]-009) and 2006 (grant H18-jyunkannki[seishuu]-ippan-018); and Health and Labour Science Research Grants for research on medical devices for analyzing, supporting, and substituting the function of human body in 2005 (grant H17-physi-002).

* Corresponding author. Tel.: +81-463-931-121; fax: +81-463-936-684.
E-mail address: fukuyama@is.icc.u-tokai.ac.jp (N. Fukuyama).

0899-9007/07/$ – see front matter © 2007 Elsevier Inc. All rights reserved.
doi:10.1016/j.nut.2006.10.004

Introduction

In Japan, rice vinegar is widely used in the preparation of Sushi or Kaisekiryouri. It is known to have a bactericidal action and an orexigenic action and was reported to have a preventive effect against hypertension and arterial sclerosis [1]. Recently, rice vinegar that has been matured and fermented for many years in earthenware jars has attracted attention as a health food. The supernatant is known as Korozu, and the solid residue of the production process, Kurozu moromimatsu (Kurozu-M), is rich in organic materials and minerals. However, the effect of Kurozu-M on disease has not yet been examined.

Colorectal cancer accounts for >90% of malignant tumors of the large intestine and is the third most common cause of death from malignant disease in the Western world [2]. It was reported that ethyl acetate extract of Kurozu inhibited carcinogenesis in azoxymethane-treated rats [3] and caused G0/G1 arrest through p21 induction in Caco-2 cells [4]. It is known that active oxygen species activate metalloproteinases (MMPs) in colon cancer tissue, leading to destruction of the basal membrane [5], thereby promoting distant metastasis. However, the effects of Kurozu on active oxygen production and MMP activation are unknown.

In this study, we examined the direct effects of Kurozu and Kurozu-M on human colon cancer cells (DLD cells, well-differentiated adenocarcinoma; Lovo cells, poorly differentiated adenocarcinoma) transplanted into nude mice and found that both inhibited tumor growth. We also examined the mechanisms involved, focusing on active oxygen production and MMP activation. Because direct measurement of active oxygen production in tissues is difficult, we used an indirect method based on staining for nitrotyrosine, the formation of which involves active oxygen.

Materials and methods

Preparation of Kurozu and Kurozu-M diets

The Kurozu and Kurozu-M diets were obtained from Sakamotojyozo Co., Ltd. (Kagoshima, Japan). The Kurozu diet included 0.32% 10-fold–concentrated Kurozu, and the Kurozu-M diet included 2% Kurozu moromimatsu powder in CE-2 basic rodent diet (Nihon CLEA Co., Ltd, Tokyo, Japan).

Preparation of animal model

Lovo and DLD cells were maintained under the conditions recommended by the supplier. Four-week-old to 6-wk-old female nude mice were maintained in a pathogen-free environment and handled according to the university's guidelines for animal care and use.

Female nu/nu mice were injected with 1×10^6 Lovo cells or DLD cells into the right flank. The tumors reached 5–10 mm in diameter at about 6 wk after injection in the control group on a standard CE-2 diet. The CE-2, Kurozu, or Kurozu-M diet was supplied from 1 wk before cancer cell injection.

Measurement of subcutaneous tumor

Tumor dimensions were measured with a linear caliper every 2 or 3 days for one month. We measured the major axis and the tumor volume, which was calculated using the equation $V\ (mm^3) = a \times b^2$, where a is the largest dimension and and b is the perpendicular diameter.

Hematoxylin-eosin staining, terminal deoxynucleotidyl transferase-mediated dUTP nick end-labeling staining, and nitrotyrosine immunostaining

At the end of the experiment, tumor tissue was fixed with 4% paraformaldehyde and sectioned. Hematoxylin-eosin (HE) staining was performed with conventional methods. Terminal deoxynucleotidyl transferase-mediated dUTP nick end-labeling (TUNEL) staining was performed according to the kit manufacturer's instructions, and apoptosis was visualized as brown staining, located in the nucleus. Apoptotic cells were counted in 10 fields of each slide under a 40× microscope.

For nitrotyrosine staining, endogenous peroxidase in sections was quenched with 0.3% H_2O_2 in 60% methanol for 30 min. The sections were permeabilized with 0.1% Triton X-100 in phosphate buffered saline (PBS) for 20 min. Nonspecific adsorption was minimized by incubating the sections in 2% normal goat serum in PBS for 20 min. Sections were incubated overnight with anti-nitrotyrosine rabbit polyclonal antibody (1:500 in PBS), and specific labeling was detected with diaminobenzidine tetrahydrochloride. To verify the binding specificity to nitrotyrosine, some sections were incubated with primary antibody only (no secondary antibody) or with secondary antibody only (no primary antibody). No positive staining was found in these sections, indicating that the immunoreaction was specific. Some sections were incubated with the primary antibody (anti-nitrotyrosine) in the presence of excess nitrotyrosine (10 mM) to further verify the binding specificity.

MMP-2 and MMP-9 assays

Levels of total MMP-2 and MMP-9 and endogenous activated MMP-2 and MMP-9 were assayed with commercial assay kits (Amersham Pharmacia Biotech, Buckinghamshire, UK).

MMP-2 assay

Eight weeks after injection of Lovo cells, tumors were removed. Tissues were homogenized in 50 mM Tris-HCl buffer (pH 7.4) containing 1 mM monothioglycerol and